January 2014

# Metal Enhanced Fluorescence With Gold Nanoparticles

Shaina Larissa Strating Mattingly

METAL ENHANCED FLUORESCENCE WITH GOLD NANOPARTICLES

by

Shaina LaRissa Strating Mattingly

Bachelor of Science, University of North Dakota, 2011

A Thesis

Submitted to the Graduate Faculty

of the

University of North Dakota

in partial fulfillment of the requirements

for the degree of

Master of Science

Grand Forks, North Dakota

August 2014

This thesis, submitted by Shaina LaRissa Strating Mattingly in partial fulfillment of the requirements for the Degree of Master of Science from the University of North Dakota, has been read by the Facultee Advisory Committee under whom the work has been done and is hereby approved.

_____
Julia Zhao

_____
David Pierce

_____
Alena Kubatova

This thesis is being submitted by the appointed advisory committee as having met all of the requirements of the School of Graduate Studies at the University of North Dakota and is hereby approved.

_____
Wayne Swisher,
Dean of the School of Graduate Studies

_____
Date

PERMISSION

Title                Metal Enhanced Fluorescence with Gold Nanoparticles

Department     Chemistry

Degree        Master of Science

In presenting this thesis in partial fulfillment of the requirements for a graduate degree from the University of North Dakota, I agree that the library of this University shall make it freely available for inspection. I further agree that permission for extensive copying for scholarly purposes may be granted by the professor who supervised my thesis work or, in her absence, by the Chairperson of the department or the dean of the School of Graduate Studies. It is understood that any copying or publication or other use of this thesis or part thereof for financial gain shall not be allowed without my written permission. It is also understood that due recognition shall be given to me and to the University of North Dakota in any scholarly use which may be made of any material in my thesis.

Shaina LaRissa Strating Mattingly

24 July 2014

TABLE OF CONTENTS

# LIST OF FIGURES

# LIST OF TABLES

ACKNOWLEDGMENTS

I express my gratitude to my committee members and advisor for their guidance during my time as a student in the UND Chemistry Department.

ABSTRACT

A novel hybrid nanocomposite of Au nanoparticle-modified silicon nanowire was developed for surface enhanced fluorescence applications. The designed nanocomposite contained a silicon nanowire, gold nanoparticles and a silica layer doped with dye molecules. The hybrid nanomaterial was characterized using scanning electron microscopy (SEM), scanning transmission electron microscopy (STEM), fluorescence measurements, Fourier transform infrared (FT-IR) spectroscopy, and energy-dispersive X-ray spectroscopy (EDS). The results showed that the gold nanoparticles were uniformly adhered on the silicon nanowires and covered by a thin silica layer. The nanostructure exhibited strong capacity for surface enhanced fluorescence. Different enhancement factors were obtained by changing synthetic conditions.

The second goal of the project was to determine if the shape of gold nanoparticles affects the extent of its fluorescence enhancement under constant external factors. Two shapes of gold nanoparticles were synthesized and characterized by SEM, STEM, zeta potential and absorbance measurements. Then they were coated with fluorescent dye-doped silica and the fluorescence intensity was measured and compared to the pure fluorescent dye. Gold nanorods enhanced fluorescence more than gold nanostars and that the fluorescent dye Alexafluor 700 showed a greater fluorescence intensity change in the presence of nanoparticles than methylene blue.

CHAPTER 1

Gold Nanoparticle-Silicon Nanowire Composites for Surface Enhanced Fluorescence

1.1 Introduction

Surface enhanced fluorescence (SEF) is a phenomenon that leads to increased

fluorescence signal. SEF can contribute to more sensitive imaging with fewer fluorescent

materials needed. Nano-scale objects lend their unique optical and electronic properties

to make ideal SEF structures. In this project, silicon nanowires and gold nanoparticles

were used to construct a novel SEF structure.

Each component of the structure affects the degree to which fluorescence can be

enhanced. The two main phenomena that lead to enhancement are surface plasmon

resonance and surface enhanced fluorescence.

1.1.1 Surface Enhanced Fluorescence

Electrons absorb energy and are promoted to excited states. When the electrons

relax back to their original ground state energy level, they emit radiation of a wavelength

that is related to the energy of the excited state through Equation 1.

Equation 1

$$E = hc/\lambda$$

Where E is the energy, h is Plank's constant, c is the speed of light in a vacuum, and $\lambda$ is

the wavelength of emitted radiation. If the electrons are excited by electromagnetic

radiation to a singlet state and then relax to their ground state and emit light of a longer

1

wavelength than that which was absorbed, the process is called fluorescence.[1]

Fluorescence can be represented by a Jabłoński diagram, an example of which is shown

in Figure 1.1.
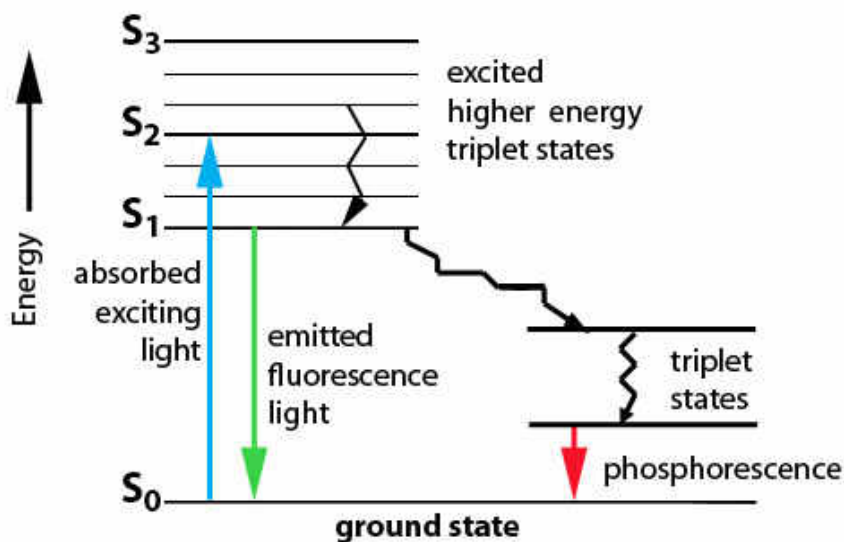


**Figure 1.1** A Jabłoński diagram showing the processes of absorption, fluorescence and phosphorescence. $S_0$ is the ground energy singlet state. $S_1$, $S_2$, and $S_3$ are the excited singlet states. From reference 3.

Fluorescence often occurs in molecules with delocalized $\pi$ bonds when the electrons are

excited from a bonding $\pi$ orbital to an antibonding $\pi$ orbital.

Surface enhanced fluorescence (SEF) results from the process of controlling the

surface of a structure to allow the maximum intensity of fluorescence from the surface to

reach a light detector. SEF relies on the manipulation of the local environment of a

fluorophore to maximize the radiative relaxation rate compared to the same fluorophore

in free space. Other competitive, non-radiative processes must be nearly eliminated.[1]

LSPR is one of the most important factors employed for SEF. Other factors that influence

SEF are differences in the dielectric constants around the fluorophore.[4] The dielectric

2

constant of silicon is $11 - 12$, silicon dioxide (silica) is 4.5 and gold is$18 - 35$.[5-6] Because

these are nanosized and not bulk materials, the values for the dielectric constants may be

significantly different.[7] However, the differences between them will still be enough to

induce SEF.

1.1.2 Surface Plasmon Resonance

　　　Surface plasmon resonance (SPR) is exhibited by metals that are highly lustrous,

such as gold, silver, copper and platinum. SPR is the result of an excited surface plasmon

of a metal. Surface plasmons are delocalized electrons that travel as waves parallel to the

surface of the metal. They can be excited by electromagnetic radiation of a specific

wavelength that strikes the metal surface at a certain incident angle, resulting in their

fluorescence emission at an angle related to the incident angle.[1] SPR enhances the

fluorescence signal because when the surface plasmon wave is emitted from the metal, it

couples with the fluorescence emission signal of a fluorophore resulting in more intense

signal. SPR can be from metallic flat, corrugated or roughened surfaces. Roughened

surfaces are also considered multi-corrugated surfaces.[2] Theoretically, the more

roughened the metal surface, the better the fluorescence enhancement.[1]

　　　Spherical metal nanoparticles provide excellent roughness for an SPR-exhibiting

device.[1] They are beneficial because multiple scattering of light occurs within the

random placement of nanoparticles on a substrate surface. Fluorescence is amplified by

propagating surface plasmon modes. In the case of highly roughened surfaces, multiple

electron scattering induces localization of surface plasmons.[1] The resonance due to

localization of surface plasmons from metal nanoparticles is a termed localized surface

plasmon resonance (LSPR) and, because of the presence of a roughened surface, it shows

3

better fluorescence enhancement than SPR from flat metallic surfaces. LSPR is only applicable to nanostructures that have a diameter much smaller than the wavelength of the incident radiation. For these particles, the electric field is mainly localized at the surface.[1]

1.1.3 Silicon Nanowires

Silicon nanowires (SiNW) are a relatively new one-dimensional nanomaterial that has been rapidly developed in recent years.[8-15] The unique advantages of this one dimensional nanomaterial include excellent electronic properties, high surface-to-volume ratio, convenient surface modification, thermo stability and biocompatibility.[16-22] SiNW arrays can be prepared reliably in a large quantity using several methods including metal-catalyzed vapor–liquid–solid (VLS), oxide-assisted growth, thermal evaporation with a catalyst, and wet chemical methods.[8,23-29] The applications of the SiNWs have been realized in several fields, such as electrical devices, solar cells, drug delivery and biosensors.[13,21,30-34] For example, Chen and coworkers have developed SiNWs as lithium battery anodes[35], and Xie *et al.* recently doped SiNWs into graphene nanoribbons to enhance the performance of Schottky solar cells.[36]

Moreover, the surface of SiNWs can be modified and grafted with various functional groups to advance their applications.[18,37,38] Their unique morphology and large aspect ratio make SiNWs a good substrate candidate for preparing nanocomposites.

Nanowires are defined as objects with a diameter in the tens of nanometers and an unrestricted length range. They have even been reported with a length of hundreds of meters[39] and their synthesis is well documented.[40-46]

4

Silicon is a semiconductor, which means its conductivity increases with increasing temperature.  A conductor, semiconductor or insulator can be determined by the energy of its band gap.  The higher the energy, the less conducting the material is.  For example, diamond is an insulator with a band gap of 5.5 eV at 302 K. The conductor, Indium (III) nitride, has a band gap of 0.7 eV at 302 K.  Silicon has a band gap value of 1.11 eV at 302 K, intermediate of conductors and insulators.[47] Pairing a semiconductor with a plasmonic metal is advantageous.  When gold nanoparticles are deposited on a semiconductor surface the surface plasmon resonance enhances the optical absorption and photocurrent generated by the semiconductor.[48]

1.1.4 Gold Nanoparticles

The main advantage of gold nanoparticles (AuNP) in this work is their LSPR. Characteristics of LSPR can be manipulated by changing the size of the AuNP. Nanoparticles that are too small (< 2 nm) do not have surface plasmons due to quantum confinement effects.[49] An important aspect of having AuNP adjacent to each other on the SiNW surface is their ability to couple their LSPR when they are close to one another. Plasmon coupling of metal nanostructures is accompanied by color changes as a result of shifts in their scattering spectral peaks.  The coupling-induced plasmon shift decays exponentially as the particle spacing is decreased.[50]  Another property of AuNP that will be exploited in this work is the change in plasmon resonance frequency that results from different sizes of AuNP.  Generally, the plasmon red shifts and broadens with increasing AuNP size.[51]

Nanocomposites usually contain a substrate nanomaterial and some functional species. Various nanocomposites have been developed for a wide variety of

5

applications.[15,52-54] Surface enhanced fluorescence (SEF) is one of the popular application fields for nanocomposites.[33,55,56] A number of SEF nanocomposites have been fabricated based on the unique optical and electronic properties of nanomaterials.[57-59] In a traditional SEF nanocomposite, noble metal nanoparticles are employed to exhibit localized surface plasmon resonance (LSPR) which occurs on flat, corrugated or roughened surfaces of substrate nanomaterials.[59-61] Most of the SEF applications were performed on a planar glass substrate,[62-64] which limits their applications in biological fields. In 2004, using $SiO_2$ matrix to adjust the distance between dye molecules and silver nanoparticles, Geddes's group for the first time demonstrated a SEF platform in solutions instead of solid substrates,[65] Following this work, a number of solution-based SEF methods have been reported and expanded to Raman spectroscopy such as gold nanoparticles covered with a silica layer and shell-isolated nanoparticle-enhanced Raman spectroscopy.[66,67] To our knowledge, SEF on one dimensional nanosubstrates has not been well studied. The exploration of SiNWs as a substrate for making SEF nanocomposites may provide new insight in the field of SEF.

According to the SEF theory, when the surface plasmon resonance band of the metal nanostructure overlaps the excitation of the fluorophores localized near nanoparticles, the energy is transferred from the metal to the fluorophore so that the probability of excitation of the dye molecules is increased.[61,68] The metal nanostructure also can change the radiative deactivation rate of the fluorophores. Thus, the fluorescence lifetime and the quantum yield are changed.[69] It has been shown that fluorescence can be enhanced by 1–3 orders of magnitude when fluorophores are localized near metal nanoparticles.[70] In spite of the well-developed SEF mechanisms, the geometric and

6

dimensional effects of the nanosubstrates on the SEF efficiency or on fluorescent molecular properties have not been well understood. Therefore, the design of one-dimensional based nanocomposites for SEF may provide useful models for better understanding of the dimensional effects on the fluorescent molecular properties.

In this work, a nanocomposite was developed using 1-dimensional SiNW as the substrate for surface enhanced fluorescence. Gold nanoparticles were chosen as the SEF functional species based on their high stability and well-understood surface chemistry. In addition to the silicon nanowire and gold nanoparticles, the designed nanocomposites contained a silica layer doped with dye molecules. The nanocomposites were evaluated to to see if they enhance the surface fluorescence. It is expected that the 1-dimensional nanocomposite might be used for studying dimensional effects on SEF.

1.2 Experimental

1.2.1 Materials and Instrumentation

Gold (III) chloride trihydrate ($HAuCl_4$), sodium citrate ($Na_3C_6H_5O_7$) and (3-aminopropyl)triethoxysilane (APTES) were purchased from Sigma-Aldrich (St. Louis, MO). Sodium silicate and phosphate buffered saline (PBS) tablets were purchased from Fisher (Waltham, MA). Tris(bipyridine)ruthenium (II) chloride ($[Ru(bpy)_3]Cl_2$) was purchased from Acros Organics (Thermo Fisher Scientific Inc., NJ). Deionized (D.I.) water was obtained from a Millipore water purification system and had a resistivity of 18.2 MΩ•cm (EMD Millipore, Billerica, MA). PBS buffer (pH = 7.4 at 25 ºC) was prepared by dissolving one PBS tablet into 200 mL water.

Scanning electron microscopy images were taken with a Hitachi SU 8010 field emission scanning electron microscope (FE-SEM, Hitachi High Technologies America,

Inc., Schaumburg, IL).  The energy dispersive X-ray spectroscopy spectra were obtained using an X-Max instrument (Oxford Instruments, Scotts Valley, CA). Samples were separated via centrifugation in an Eppendorf Centrifuge 5804 (Hauppauge, NY). Dynamic light scattering measurements were conducted on a Malvern Zetasizer Nano Series instrument (Worcestershire, UK). Fluorescence measurements were performed using a Fluorolog-3 spectrofluorometer equipped with a 450 W xenon lamp (Horiba Scientific, Irvine CA).

### 1.2.2 Synthesis of Silicon Nanowires

Silicon nanowires were provided by Nanosys (Palo Alto, CA). They were synthesized  according to company protocol by high temperature chemical vapor deposition. In this procedure, a gold catalyst was deposited onto stainless steel and placed into a CVD reactor with silicon tetrahydride as the growth gas.  After growth, the silicon nanowires were washed with water and alcohol by sonication.[71]

### 1.2.3 Synthesis of Gold Nanoparticles

Gold nanoparticles were synthesized using the citrate reduction method.[72,73] A 50.0 mL aliquot of 0.01% $HAuCl_4$ was added to a round-bottomed flask and heated under reflux until boiling. Afterwards, 2.0 mL fresh prepared sodium citrate solution (1.0% w/v) was added with stirring. The solution was kept boiling for 10 min after the color turned red, which indicated the gold nanoparticles were formed. The as-synthesized gold nanoparticles were used without further purification. The size of gold nanoparticles was measured to be 16.7 nm ± 3 nm using the Zetasizer with a concentration of 0.1 mg/mL.

### 1.2.4 Hybridization of Silicon Nanowires with Gold Nanoparticles

A 10 mg sample of SiNW was heated at 550 ℃ for one hour. After heating, the SiNW were added to 10.0 mL of 1% $NH_4OH$ solution and sonicated for 30 min. Then 5.0 mL of this SiNW solution was added into 45.0 mL of acetone and 1.0 mL of APTES was added dropwise under vigorous stirring for one hour.[24] The sample was washed twice with acetone and once with water and separated by centrifugation (10,000 rpm for 20 min). Finally the sample was weighed and diluted with water to a concentration of 1.0 mg/mL SiNW. In a typical experiment, 1.0 mL of as-synthesized AuNP were mixed with 1.0 mL of SiNW under sonication for 30 min. The AuNP would attach to the surface of SiNW to form AuNP-SiNW hybrids due to electrostatic attraction; the free AuNP were washed away through centrifugation.

### 1.2.5 Doping Dye Molecules to the Hybrids

The obtained AuNP-SiNW hybrids were used as a substrate for doping dye molecules. A silica layer was grown on the surface of the hybrid. During this growth, dye molecules were doped into the silica layer. In a typical experiment, 1.0 mg AuNP-SiNW was added to 30.0 mL of water and sonicated to ensure the AuNP-SiNW were well dispersed. Then 3.0 mL of fresh 0.1 mM APTES was added into the solution and stirred for 10 min. Afterwards, 4.5 mL of 0.54% wt. sodium silicate was added into the solution and the solution was placed in a water bath at 90 ℃. After 20 min of incubation, 0.2 mL of 0.01 M $[Ru(bpy)_3]Cl_2$/PBS solution was added and the solution was kept at 90 ℃ for 2 h. The samples were allowed to cool and washed 3 times with water and separated from the solution by centrifugation (11,000 rpm for 25 min). The final product was dissolved in 1.0 mL of D.I. water.

1.2.6 Release Dye Molecules from the Nanocomposites

The silica layer can be dissolved in a high concentration of NaOH to release the dye molecules. In a typical experiment, 0.1 mL of 0.4 M NaOH was added into 0.5 mL of dye-doped AuNP-SiNW solution. After stirring overnight, the silica layer was dissolved, and the AuNP and SiNW were removed by centrifugation. Thus the dye molecules were released into the supernatant. Finally, 0.1 mL of 0.4 M $HNO_3$ was added to neutralize the pH.

1.2.7 Detection of Fluorescence of Dye Molecules

Fluorescence measurements were performed using a Fluorolog-3 spectrofluorometer equipped with a 450 W xenon lamp. The pH value of all samples was adjusted to 7 with PBS buffer. For $[Ru(bpy)_3]Cl_2$, excitation was set to 488 nm and emission wavelength range was 500 – 700 nm. Slit width was set at 2 nm for all measurements.

1.3 Results and Discussion

1.3.1 Design of the Nanocomposite

The goal of this design was to controllably assemble AuNP on a 1D nanosized substrate to avoid AuNP aggregation, which tends to occur to AuNP in solution.[74] Aggregation limits their SEF efficiency and potential applications in biological environments. Several factors should be considered when choosing substrate materials such as high surface area and easy surface modification for AuNP loading, as well as chemical and physical inertness and stability to avoid affecting SEF. Based on these considerations, one-dimensional silicon nanowires were selected as the substrate.[33,34] The

AuNP on SiNW were further coated with silica layer containing dye molecules for studying SEF. The schematic diagram for synthesizing the nanocomposite is shown in Figure 1.2. A modified silicon nanowire was employed as the substrate after cleaning (Figure 1.2 A). Gold nanoparticles were immobilized on the surface of the SiNW (Figure 1.2 B). The distances between the AuNPs could be adjusted by changing the ratio of AuNP to SiNWs for an optimal SEF effect.[75] Then a layer of silica was grown initially on the AuNP-SiNW surface as the spacer to avoid quenching effect of AuNP to dye molecules. The subsequent silica layer was doped with fluorescent molecules (Figure 1.2 C).
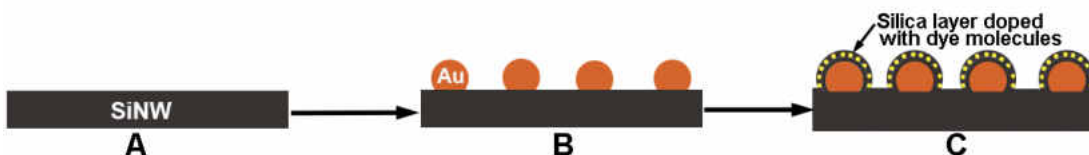


**Figure 1.2** Schematic diagram of an AuNPs-SiNW nanocomposite: (A) SiNW; (B) the SiNW coated with AuNP; (C) AuNP-SiNW covered by the silica layer doped with dye molecules; a layer of silica was first grown on the AuNP as a spacer before dye doping. The yellow dots around the AuNP represent dye molecules.

1.3.2 Surface Modification of SiNWs

The SiNWs were cleaned and modified for coating with AuNP. The removal of impurities was accomplished by heating to 550 °C as described in Section 1.2.4. Figure 1.3 (A) is the SEM image of pure SiNWs, showing their uniform size with a diameter of 40 - 50 nm and a length of 10 μm. The surface of the nanowires was smooth, as seen in Figure 1.3 (A), which was ideal for further modification.

To assemble AuNP on the SiNW, the surface of SiNW was modified to become positively charged. Thus, by electrostatic attraction, the negatively charged citrate-capped

AuNP would be attracted to the SiNW surface. The positively charged SiNW surface was obtained by reacting with APTES for adding positively charged amino groups to the SiNW surface.
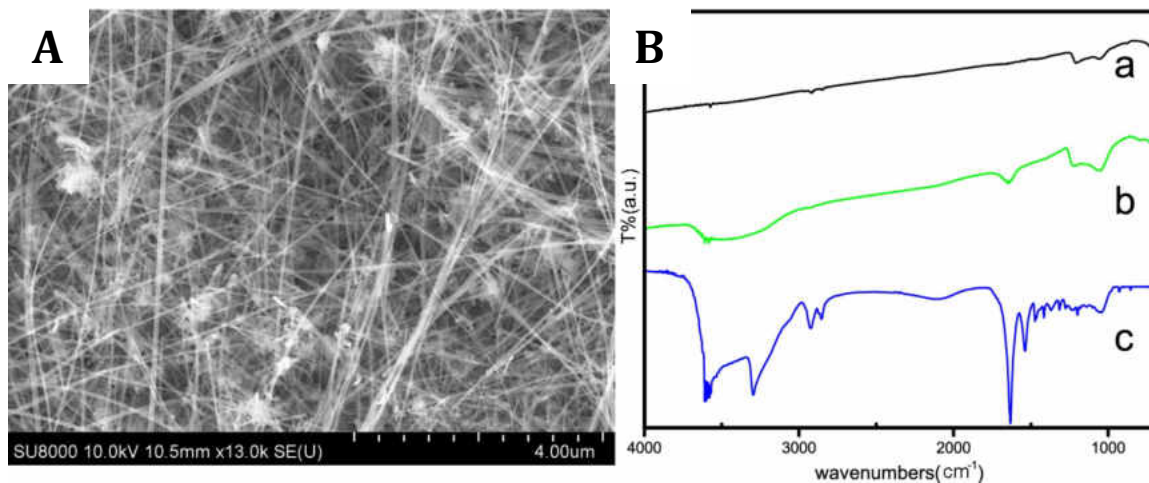


**Figure 1.3** (A) SEM image of pure SiNW. (B) FTIR spectra of samples: pure SiNW (a); SiNW after NH$_4$OH treatment (b); SiNW after APTES treatment (c).

The surface modification of SiNW was first confirmed using FT-IR spectroscopy. Figure 1.3 (B) shows the changes of SiNW during the surface modification process. Figure 1.3 (B) curve (a) represents the cleaned SiNW after heating, which has small peaks at around 1000 cm$^{-1}$ showing Si-O bands on the surface. After treatment using NH$_4$OH, hydroxyl groups were generated on the SiNW surface. The –OH group can be confirmed by the broad peak at 3500 cm$^{-1}$ in curve (b). After reaction with APTES, new peaks appeared at 3300 and 2900 cm$^{-1}$ as shown in curve (c), representing N-H and C-H bonds, respectively. This result confirmed that amino groups were grafted on the surface of SiNWs through hydrolysis of APTES. The peaks near 2900 cm$^{-1}$ correspond to the methyl and methylene groups of APTES.

12

In addition to FT-IR, the zeta potential of the SiNW was measured during the

surface modification process. Pure SiNW showed a zeta potential of -30.1 mV.  After the

NH₄OH treatment, the zeta potential became -44.70 mV signifying that -OH groups were

generated on the surface and caused the nanowire to become more negatively charged.

After the APTES treatment, the zeta potential became -0.325 mV. The increase of surface

zeta potential to a more positive value represented that the -OH groups reacted with

APTES during the hydrolysis and the -NH$_2$ became -NH$_3$$^+$ by absorbing a proton. The

reactions are shown in Figure 1.4.
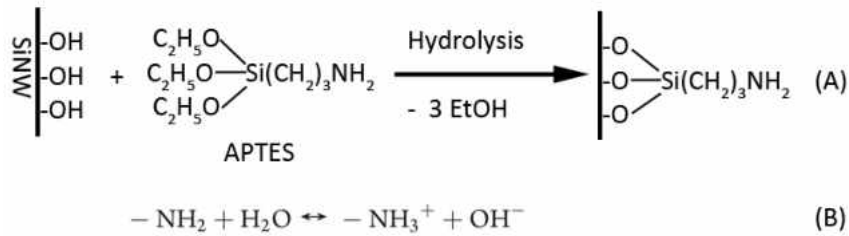


**Figure 1.4** (A) Reaction of APTES with hydroxyl groups on SiNW surface.  (B)
Protonation of amine group by water.

1.3.3 Attachment of AuNP to SiNW

The AuNP-SiNW were formed based on electrostatic attraction between amino

groups and AuNPs. Gold nanoparticles produced from citrate reduction were negatively

charged due to the citrate ions on their surface. The zeta potential measurement of as-

synthesized AuNPs showed a value of -30.9 mV, which confirmed the negative charge.

Therefore, the amine modified SiNWs were directly mixed with AuNP solution to form

AuNP-SiNW. This step was performed under sonication to avoid aggregation during the

reaction. Figure 1.5 (A) is the SEM image showing that AuNP were uniformly assembled on the SiNW surface.

Elemental analysis was performed to further verify the existence of gold nanoparticles on the SiNWs. As shown in the EDS spectra (Figure 1.5 B), the gold peaks can be found in the sample spectra between 2 and 2.15 keV. The C and O in the EDS spectra come from the hydrolyzed APTES and oxidized layer of silicon nanowires.
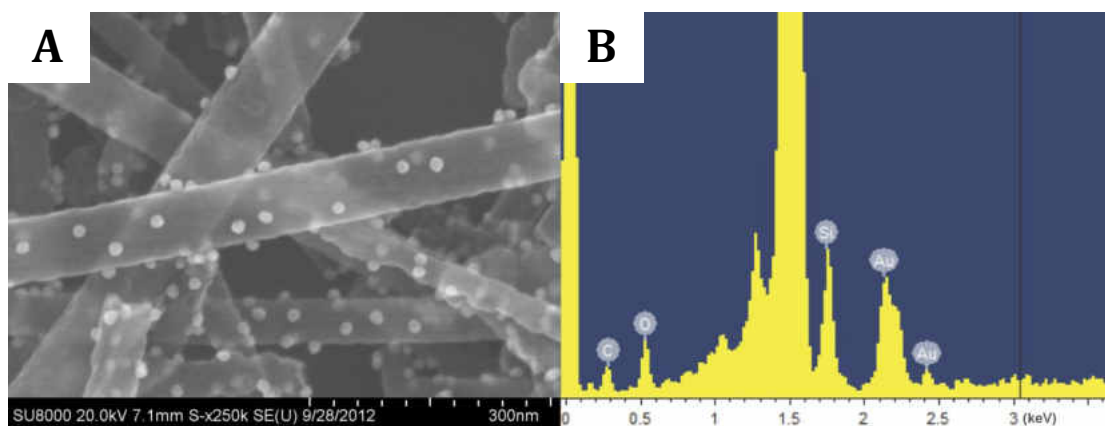


**Figure 1.5** (A) SEM image of AuNP-SiNW. (B) Elemental analysis of AuNP-SiNW.

1.3.4 Formation of Silica Layer on the Nanocomposite

In order to investigate SEF effects on the 1D nanocomposite, the synthesized AuNP-SiNW was applied as a nanosubstrate and dye molecules were added to the nanocomposite. To avoid the quenching effect of the AuNPs to fluorescent dye molecules, a distance between the dye molecules and AuNPs is needed. In the design a thin silica layer was employed to perform this role. By adding sodium silicate[55] into AuNP-SiNW solution, a silica layer was formed on the nanocomposite surface. Figure 1.6 (A) is the SEM image of the nanocomposite with the silica layer. Compared to

Figure 1.5 (A) without the silica layer, the morphology of the nanocomposite changed slightly. A semi-transparent layer was found around the gold nanoparticles to form a core-shell structure while the gold nanoparticles remained in their original positions throughout the reaction. Further, an STEM image of the sample is shown in Figure 1.6 (B). In this image the gold nanoparticles appeared as black dots and SiNW showed a grey color. On the surface of SiNW, a layer with a light grey color was observed clearly, which represents the silica layer. An enlarged STEM image (Figure 1.6 (B), inset) indicated that the AuNP-SiNW structure was covered by the silica layer.

To further confirm the silica layer on the surface of the nanocomposite, the nanocomposite with and without the silica layer was heated at 550 ºC for one hour. Metal nanoparticles are not stable at high temperatures. Gold nanoparticles form aggregates at high temperatures. Figure 1.6 (C) and Figure 1.6 (D) are SEM images of heated bare AuNP-SiNW and AuNP-SiNW with a silica layer, respectively. Large gold aggregates on the bare AuNP-SiNW were found in Figure 1.6 (C). In contrast, the gold nanoparticles in Figure 1.6 (D) remained isolated through the heating process. It was concluded that the stability of the AuNPs at high temperatures is due to the presence of the silica layer.
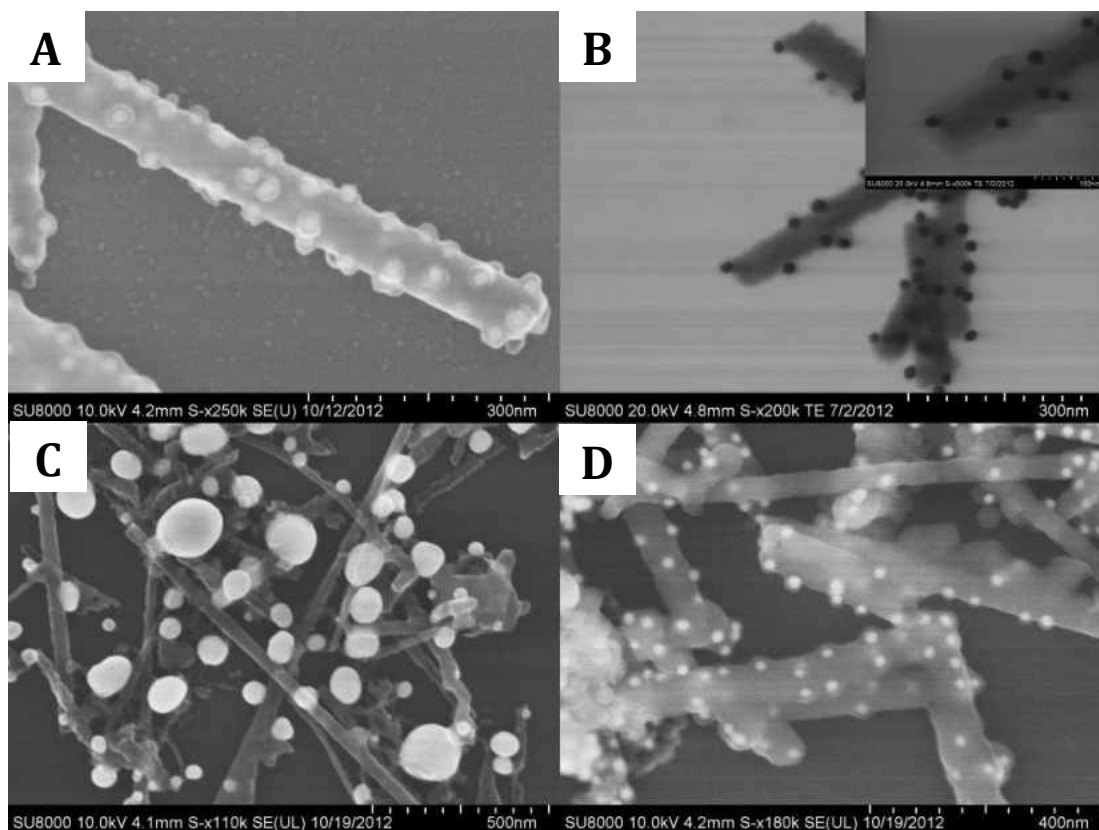
**Figure 1.6** SEM images of samples: (A) AuNP-SiNW with silica layer; (B) STEM image of AuNP-SiNW with silica layer; (C) Bare AuNP-SiNW after heating at 550 ºC for one hour; (D) AuNP-SiNW with silica layer after heating at 550 ºC for one hour.

1.3.5 Doping Dye Molecules into the AuNP-SiNW Nanocomposites.

The AuNP-SiNW nanocomposites were combined with sodium silicate and APTES as mentioned in Section 1.3.4, allowing for formation of a silica layer on the surface of the nanocomposites. After the reaction was allowed to take place for 50 min, [Ru(bpy)$_3$]Cl$_2$ was added to the reaction solution. Therefore, the additional silica layer grown on the surface was doped with [Ru(bpy)$_3$]Cl$_2$. From Figure 1.6 (B), the thickness of the silica layer was about 20 nm after 2 h growth time. The thickness of the spacer silica layer with 50 min growth time was about 10 nm, which is enough to avoid fluorescence quenching of dye from AuNP.

16

1.3.6 Surface Enhanced Fluorescence Evaluation

The SEF effect of the developed nanocomposite was investigated through a series of fluorescence measurements. First, 1.0 mL of 1.0 mg/mL AuNPs-SiNWs with no silica layer was directly added into 1.0 mL of 0.01 M [Ru(bpy)$_3$]Cl$_2$ PBS solution. Compared with the fluorescence intensity of pure [Ru(bpy)$_3$]Cl$_2$ solution diluted by 1.0 mL water (Figure 1.7 (A) curve a), the fluorescence signal from the [Ru(bpy)$_3$]Cl$_2$ solution containing AuNP-SiNW (Figure 1.7 (A) curve b) was reduced by 12% at 610 nm. This seems to be due to the quenching effect of AuNPs to dye molecules when they were in close proximity. Based on the literature,[55] the distance between dye molecules and the metal surface is crucial. When the distance is less than 10 nm, the fluorescence will be quenched. In the mixed solution, free dye molecules would be adsorbed onto the AuNPs-SiNW so that the fluorescence signal would became weaker.

Next fluorescence signal of different nanocomposites with or without dye was detected. A series of comparisons is shown in Figure 1.7 (B). The pure SiNWs (Figure 1.7 (B) curve a) and AuNP-SiNW (Figure 1.7 (B) curve b) showed no detectable fluorescence signal due to the absence of the fluorophore. After dye molecules were doped into the silica layer on SiNWs (Figure 1.7 (B) curve c), an emission peak appeared on the fluorescence spectrum,  meaning that [Ru(bpy)$_3$]Cl$_2$ was doped into the silica layer. However, when the same amount of dye molecules were doped into the silica layer on the AuNPs-SiNW, the fluorescence signal increased dramatically (Figure 1.7 (B) curve d). The difference in fluorescence came from the enhancement caused by AuNPs interacting with dye molecules on the SiNW.
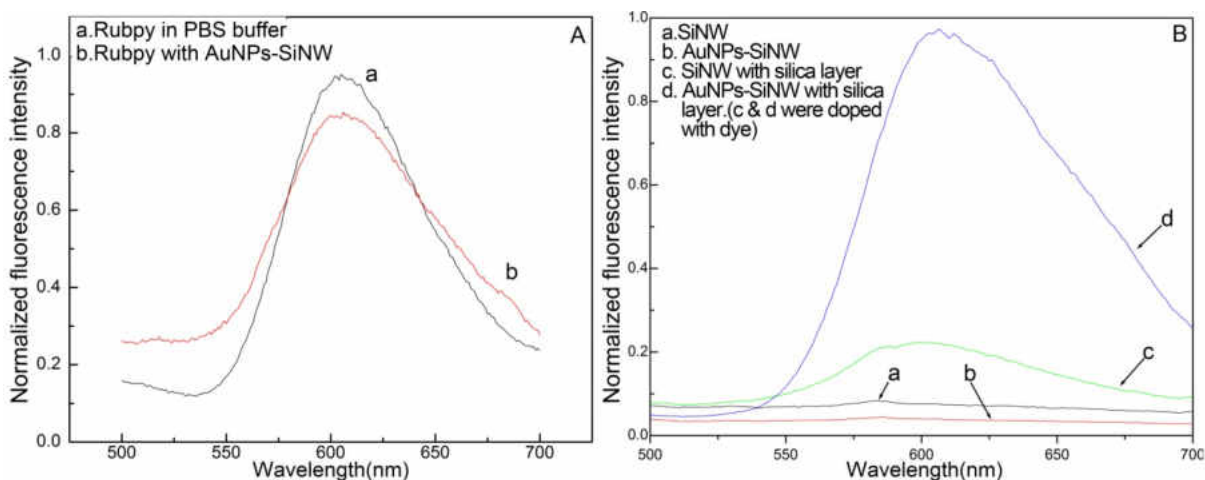
**Figure 1.7** (A) Fluorescence spectra of pure [Ru(bpy)$_3$]Cl$_2$ solution (0.01 M) (a) and [Ru(bpy)$_3$]Cl$_2$ with AuNPs-SiNW solution (b); (B) Fluorescence spectra of nanomaterials: (a) SiNWs (0.1 mg/mL); (b) AuNPs-SiNW(0.1 mg/mL); (c) SiNWs with silica layer (0.1 mg/mL); (d) AuNPs-SiNWs with silica layer (0.1 mg/mL). [Ru(bpy)$_3$]Cl$_2$(0.01 M) was doped into silica layer as a fluorophore for sample c and d during synthesis. All solutions were adjusted to pH 7.4 at 25 ºC with PBS.

1.3.7 Optimization of the Enhancement Factor

In order to obtain higher fluorescence enhancement, different densities of gold nanoparticles were assembled on the SiNWs. SiNW (1.0 mL of 1.0 mg/mL) were combined in solution with different volumes (0.1, 0.5 and 1.0 mL) of AuNP solution (0.6 mg/mL), different densities of AuNPs on the SiNWs were obtained. As shown in Figure 1.8 (A), sample A only has 1 - 2 nanoparticles formed on every 500 nm of SiNWs when the weight ratio of AuNP to SiNW was 0.06. As the amount of AuNP increased by 5 times, the assembled AuNPs on the SiNWs increased significantly. Sample B has around 5 - 7 NPs on every 500 nm of nanowire when the weight ratio was 0.3 (Figure 1.8 B). Further increasing the weight ratio of AuNP to SiNW to 0.6, 12-16 NPs on every 500 nm of nanowire was found (sample C, Figure 1.8 C). These results indicated that there is a direct relationship between the concentration of AuNPs and the final amounts of AuNPs attached to SiNW surface. Therefore, the amount of AuNPs on the SiNWs was tunable.

18

The different densities of AuNPs on the nanocomposites could affect the fluorescence enhancement factor.
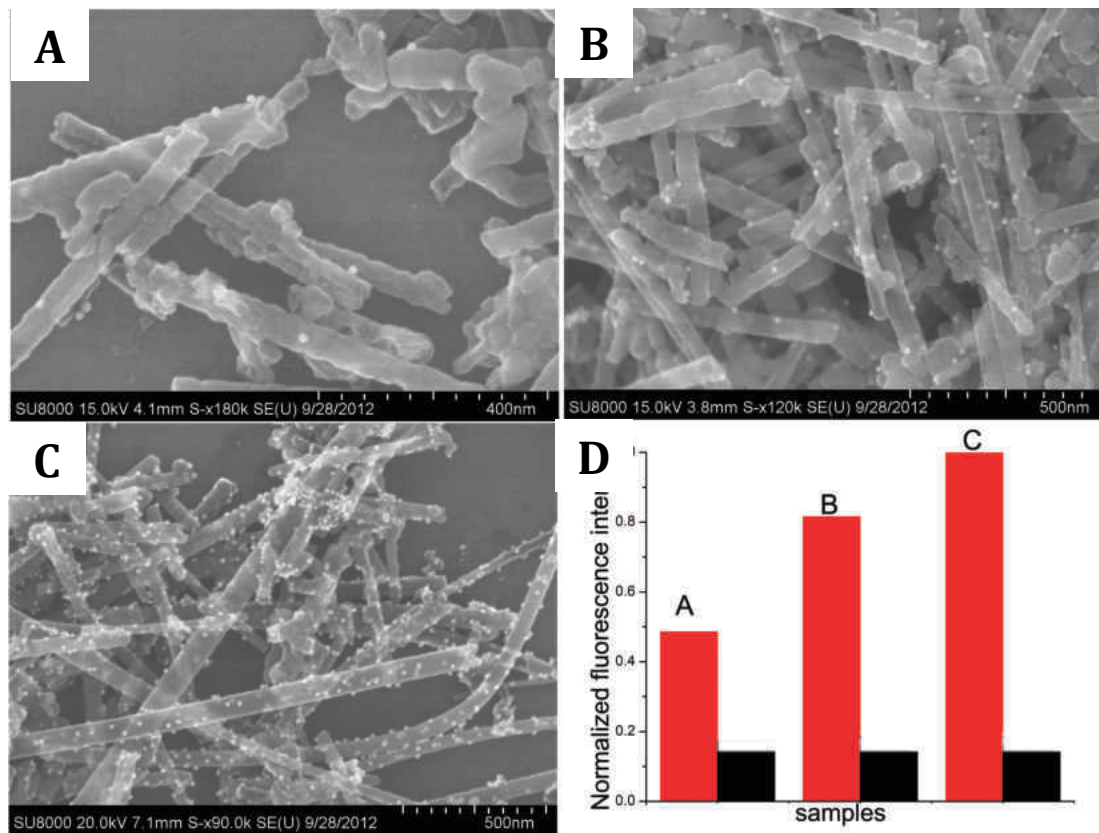


**Figure 1.8** A, B and C are SEM images of AuNPs-SiNWs. 1.0 mL of 1.0 mg/mL SiNW solution mixed with different volumes (0.1, 0.5 and 1.0 mL) of AuNP solution (0.6 mg/mL) to get sample A, B and C respectively. (D) Relative fluorescence intensity of nanocomposites before (red) and after (black) dissolving silica layer, signals at 610 nm were used here for calculation. The pH of samples were adjusted to 7.4 using PBS buffer.

The SEF factor was studied using the nanocomposites containing different amounts of AuNPs. The results are shown in Figure 1.8 (D). The red columns represent the fluorescence signal of AuNP-SiNW with a silica layer doped with dye molecules. The black columns represent the signal of dye released from the samples after NaOH treatment, which is the orginal fluorescence signal without any enhancment. The black

19

columns of three samples showed the same fluorescence intensity, indicating the same concentration of dye was released from the three samples. However, the red columns show different fluorescence intensities, indicating different levels of enhancement by the nanocomposites. The enhancement was characterized using fluorescence enhancement factor, F (F=$I_{nanocomposites}$/$I_{released\ dye}$, $I_{nanocomposites}$ is the fluorescence intensity of dye-doped nanocomposites; $I_{released\ dye}$ is the fluorescence intensity of released dye without AuNPs-SiNW). Using the equation, the enhancement factors of sample A, B and C were calculated to be 3.34, 5.19 and 6.42 respectively. The sample A had the fewest AuNPs on the surface, so it gave the lowest signal of all three samples and the enhancement factor was 3.34. As the number of gold nanoparticles deposited on SiNW increased, the signal became stronger with the enhancement factor of 5.19 and 6.42. During the last synthesis step, the silica layer not only covered the gold nanoparticles, but also grew on the surface of SiNW which can be clearly observed at inset of Figure 1.6 (B). Only [Ru(bpy)$_3$]Cl$_2$ molecules within the enhancement distance of gold nanoparticles are affected by the local electromagnetic field. Since the total concentration of dye was the same, the more AuNP on the SiNW surface, the larger the enhancement factor. Sample C had the highest enhancement factor and sample A had the lowest.

1.4 Conclusions

In summary, a novel nanocomposite for the surface enhanced fluorescence was developed. The nanocomposites contained silicon nanowire, gold nanoparticles and a silica layer containing dye molecules. The structure of the nanocomposites was characterized by SEM, FTIR, and EDS. Several experiments were used to optimize the parameters that would affect surface enhanced fluorescence of the nanocomposite and the

optimized parameters were utilized in characterization studies.  Fluorescence

measurements showed that the nanocomposite enhances fluorescence with an

enhancement factor of up to 6.42. By changing reaction parameters, different

enhancement factors were achieved. The nanocomposites might be applied in bioimaging

and biodetection due to the nontoxicity and stability of silica and gold.

CHAPTER 2

Surface Enhanced Fluorescence Comparison of Gold Nanorods and Gold Nanostars

2.1 Introduction

Gold nanoparticles of many shapes have been shown to enhance fluorescence based on the surface plasmon resonance (SPR) mechanism.[76] Gold nanoparticles have been successfully synthesized in many shapes including spheres (AuNP), rods (AuNR), stars (AuNS), and cubes.[77,78] The different shapes of gold nanoparticles each have different absorbance spectra in solution based on the plasmon modes of the particular shape.[85] AuNP have one absorbance peak near 530 nm;[85] AuNR have two absorbance peaks, one at 530 nm and another at a longer wavelength that is a function of AuNR aspect ratio (length:width);[86 - 89] AuNS have a broad absorbance peak that can be in the near infrared (NIR) region of the electromagnetic spectrum and is a result of the coupling of the plasmon modes of the core with those of the tips.[90]

The NIR absorbance and fluorescence enhancement effects of gold NPs have been employed for their applications as sensors. For biological imaging, the NIR region of the electromagnetic spectrum is optimum because it has good penetration, low scattering and it does not damage tissue. Therefore, gold nanoparticles are a great option to couple with fluorescent probes. Because of the different absorbance spectra of the gold nanoparticles, fluorescent probes with excitation wavelengths that overlap the

nanoparticle maximum absorbance values are chosen for optimum fluorescence enhancement.[65, 74]

The objective of the work in this chapter was to determine the fluorescence enhancement effects of two different shapes of gold nanoparticles, AuNRs, and AuNSs, to determine if one has a better fluorescence enhancement effect than the other under the same conditions. Nanoparticles were synthesized and then conjugated to fluorescently labeled DNA molecules or coated with dye-doped silica. The fluorescence of the modified nanoparticles was compared to the fluorescence of the dye alone to determine if enhancement occurred.

## 2.2 Experimental

### 2.2.1 Materials and Instrumentation

Gold (III) chloride trihydrate ($HAuCl_4$), sodium citrate and O-[2-(3-mercaptopropionylamino)ethyl]-O'-methylpolyethylene glycol (m-PEG-SH) MW 5000 were purchased from Aldrich. Sodium dodecyl sulfate (SDS) was purchased from MP Biomedicals. Dithiothreitol (DTT), cetyltrimethylammonium bromide (CTAB), hydroxylamine, silver nitrate, sodium borohydride, ascorbic acid and ethanol were obtained from Fisher Scientific. Alexafluor 700 and custom-sequence single stranded DNA (ssDNA) labeled with Alexafluor 532 and Alexafluor 750 were purchased from Invitrogen. Deionized water was obtained from a Millipore water purification system and had a resistivity of 18.2 MΩ•cm (EMD Millipore, Billerica, MA).

Fluorescence measurements were performed using a Fluorolog-3 spectrofluorometer equipped with a 450 W xenon lamp (Horiba Scientific, Irvine CA).

Scanning electron microscope and scanning transmission electron microscope (STEM) images were taken with a Hitachi SU 8010 field emission scanning electron microscope (FE-SEM, Hitachi High Technologies America, Inc., Schaumburg, IL). Samples were separated via centrifugation in an Eppendorf Centrifuge 5804 (Eppendorf, Hauppauge, NY). Dynamic light scattering and zeta potential measurements were conducted on a Malvern Zetasizer Nano Series instrument (Malvern, Worcestershire, UK).

### 2.2.2 Synthesis of AuNR

AuNR were synthesized according to Smith and Korgel.[79] A gold seed solution was prepared by adding 250 μL of 0.01 M $HAuCl_4$ to 9.75 M of 0.1 M cetyltrimethyl ammonium bromide (CTAB) solution with stirring. A growth solution was prepared by mixing 9.5 mL 0.1 M CTAB, 75 μL of 0.01 M silver nitrate, 500 μL 0.01 M $HAuCl_4$ and 55 μL of 0.1 M ascorbic acid. Next, fresh sodium borohydride (600 μL 0.01 M) was prepared by dissolving the solid sodium borohydride in ice cold water and the solution was added to the gold seeds and stirred for 2 minutes. The gold seeds were allowed to sit at room temperature for 2 hours. After 2 hours, 12 μL of the gold seed solution was added to the growth solution. The growth solution was allowed to sit at room temperature overnight. AuNRs were characterized by SEM, zeta potential measurements, and UV-Vis-NIR spectroscopy.

### 2.2.3 Synthesis of AuNS

AuNS were synthesized according to Yuan and coworkers.[78] First, silver nanoparticles were made by adding 5 mL of $2x10^{-3}$ M sodium borohydride and $38.8x10^{-3}$ M sodium citrate slowly to 50 mL of $5x10^{-3}$ M silver nitrate with vigorous stirring. The

mixture was heated to 50 °C for 30 min and then the volume was brought to 50 mL again, if needed. Next a solution of 0.5 mL of 24.3 x $10^{-3}$ M HAuCl₄ and 1.0 M 40 x $10^{-3}$ M hydroxylamine was diluted with 40 mL of Milli-Q water. Finally, 0.5 mL of the silver nanoparticles was added to the diluted solution above and stirred until the color changed from yellow to brown. AuNS were characterized by SEM, zeta potential measurements, and UV-Vis-NIR spectroscopy.

## 2.2.4 DNA Annealing

Three separate ssDNA strands were purchased. Two of the strands had the same sequence, but different fluorophores; the other was a complementary strand to them both. The sequences of the fluorophore-conjugated ssDNA and complementary ssDNA strands are shown in Figure 2.1.



**Figure 2.1** Sequence of ssDNA with fluorescent probe and the complementary ssDNA. The red fluorophore is Alexafluor 532 and the blue fluorophore is Alexafluor 750.

Figure 2.1 shows that the DNA-fluorophore conjugates have 48 base pairs, which translates to a length of about 15 nm, which is optimum for fluorescence enhancement.[80] Fluorophore ssDNA strands have a disulfide moiety at the 5' end of the DNA while the

25

florophore is at the 3' end the DNA. The disulfide bond is broken with DTT in order to form a thiol that has a strong affinity for the gold NPs. In order to anneal the fluorophore ssDNA to its complement the following procedure was applied. A 1 μM solution of fluorophore-conjugated DNA was incubated with 0.1 M DTT and 0.18 M phosphate buffer pH 7 at room temperature for 1 hour. The complementary DNA strand was diluted to 1 μM with 0.18 phosphate buffer pH 7.  Next, the two ssDNA strands were combined in equal volumes in a solution with a 0.05 M final NaCl concentration and allowed to sit at room temperature for 12 hours.[81] There are two separate fluorescent dyes because the different NPs have different maximum absorbance wavelengths.  Alexafluor 532 was used with AuNP and Alexafluor 750 was used with AuNRs and AuNSs.

2.2.5 Hybridize DNA to Nanoparticles

All NPs were washed with Milli-Q water at 10000 rpm for 20 min to a final concentration that corresponded to an optical density of 0.44 at 713 nm. To hybridize the DNA to the NPs, NaCl must be added which causes AuNP to aggregate in solution and is visually observed by the red AuNP solution changing to blue upon the addition of NaCl. To prevent aggregation of AuNP, the stabilizing agent sodium dodecyl sulfate (SDS), was added to a final concentration of 0.01 % (w/v) to all NP solutions for consistency.

To attach DNA to the surface of each NP shape, 0.44 optical density at 713 nm NP solution and 1 μM DNA solution were combined and allowed to react at room temperature for 2 h.

2.2.6 Silica Layer Growth

In a separate experiment, AuNR and AuNS were coated with a silica layer instead of hybridizing to DNA to note the fluorescence enhancement. AuNR and AuNS were first stirred overnight in a solution of m-PEG-SH.  AuNR were centrifuged at 10,000 rpm for 10 min, decanted and then resuspended in water to an absorbance intensity of 0.75 at a wavelength of 713 nm. AuNS were diluted with water to an absorbance intensity of 0.75 at 713 nm. 2 mL of 1 mM m-PEG-SH (MW 5,000) was added to both a 10 mL solution of AuNR and a 10 mL solution of AuNS.[10] Both solutions were stirred overnight at room temperature and were then centrifuged at 10,000 rpm for 25 minutes to remove excess m-PEG-SH and diluted to 3.5 mL with water. Next, silica layer growth was initiated using the modified Stöber method.[83] Twelve vessesls were prepared for the following reaction. Six reactions employed AuNR and six employed AuNS. Briefly, 0.5 mL of m-PEG-SH modified AuNR and AuNS were diluted with 3.9 mL of ethanol. Next 0.2 mL of 5% ammonia in water and 1 mL of 50 mM TEOS were added. To three reaction vessels each of AuNR and AuNS 56 μL of 0.250 M methylene blue was added. To the other three reaction vessels each of AuNR and AuNS was added 1 μL of 10 mg/mL Alexafluor 700. The reaction proceeded in the dark for 24 hours at room temperature. After 24 hours, the solutions were washed until the supernatant showed no fluorescence signal, usually 3 to 4 centrifugations at 10,000 rpm for 20 minutes.  Then the nanoparticles were resuspended in 0.5 mL ethanol. The resuspended nanoparticles (0.25 mL) were analyzed immediately for fluorescence signal. The other 0.25 mL nanoparticle solution had the silica layer dissolved to release dye into solution as described in Section 2.2.7.

2.2.7 Dissolution of Silica Layer to Release Dye

The following steps were used to dissolve the silica layer grown around the

nanoparticles to release the dye into solution.[84] Briefly, 6.67 uL of 3 M NaOH was added

to 0.25 mL dye-doped and silica-coated nanoparticles. The solutions were left for 12

hours. After 12 hours, 6.67 uL of 3 M HCl was added to each nanoparticle solution to

neutralize the NaOH and then the bare gold nanoparticles were separated from solution

by centrifugation at 10000 rpm for 30 minutes. The supernatant was collected and

analyzed for fluorescence signal.

2.3 Results and Discussion

2.3.1 AuNR and AuNS Characterization

As-prepared AuNS samples and washed AuNR samples were characterized by

SEM, UV-Vis-NIR, and particle size and zeta potential measurements.

Figure 2.2 shows the UV-Vis-NIR spectra and SEM images of bare AuNS and AuNR.
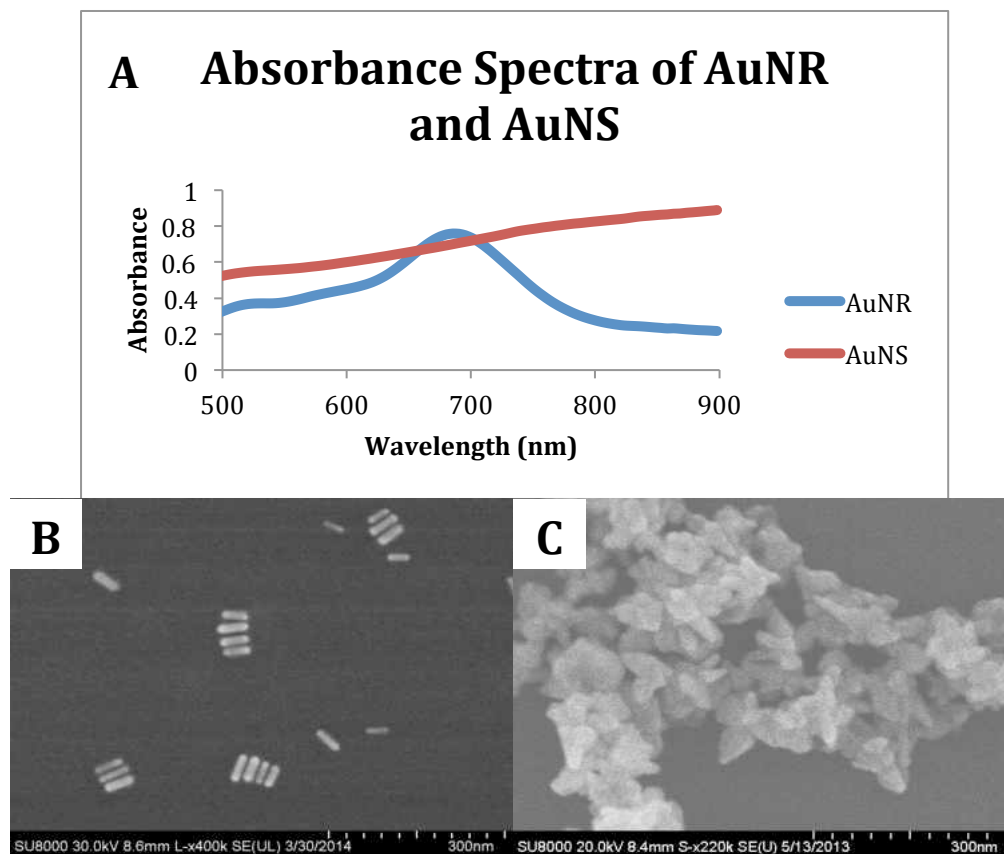
**Figure 2.2** (A) shows the absorbance spectrum of AuNR and AuNS. (B) and (C) show the SEM images of AuNR and AuNS, respectively.

The absorbance spectra of the nanoparticles shows absorbance intensity overlaps at the wavelengths 680 nm and 713 nm. The equal absorbance intensities at 713 nm were used to compare the two types of nanoparticles instead of comparing by concentrations.

Zeta potential of the nanoparticles was also measured.

Table 2.1 shows the results of these measurements.

| Sample | Zeta Potential (mV) |
|---|---|
| AuNS | -5.8 ± 4.2 |
| AuNS m-PEG-SH | -10.0 ± 8.7 |
| AuNR | 19.5 ± 15.2 |
| AuNR m-PEG-SH | 3.5 ± 12.3 |

**Table 2.1** Zeta potential of AuNS and AuNT with and without m-PEG-SH.

Table 2.1 shows that initial zeta potential of the nanoparticles is more positive than after

the addition of m-PEG-SH.  After the addition of m-PEG-SH the AuNS had an overall

negative zeta potential and the AuNR had a positive zeta potential. The zeta potential of

the nanoparticles may affect the ability for silica layer growth.

2.3.2 Silica Layer Growth

The concentration of m-PEG-SH was important to the successful growth of the

silica layer.  When the m-PEG-SH concentration was 5 nM, no fluorescence

enhancement was observed.  m-PEG-SH contains terminating hydroxyl groups that react

with TEOS to form the silica layer around the nanoparticle and ethanol as a product. If

there are not enough m-PEG-SH molecules on the nanoparticles, the silica layer does not

grow to envelop the entire nanoparticle.

2.3.3 Fluorescence Measurements

Fluorescence measurements were conducted on the dye-conjugated-DNA hybridized nanoparticles and the dye-doped silica layer nanoparticles. No conclusive fluorescence measurements were achieved with the dye-conjugated-DNA hybridized nanoparticles. This could be due to a number of factors, such as the AuNR solutions containing the strong reducing agent, $NaBH_4$, too low concentration of DNA, unoptimized hybridization conditions or aggregation of AuNPs due to the use of NaCl.

The fluorescence results with dye-doped silica coated AuNS and AuNT were promising. Fluorescence measurements were performed with a quartz crystal cuvette with 100 μL sample reservoir. Fluorescence slit width was 5 nm. Alexafluor 700 was excited at 680 nm and emission was measured from 685 to 800 nm with peak emission at 727 nm. Methylene blue was excited at  665 nm and emission was measured from 667 to 800 nm with peak emission at 674 nm. Figure 2.3 shows the fluorescence measurements of the nanoparticles before and after the silica layer was dissolved.
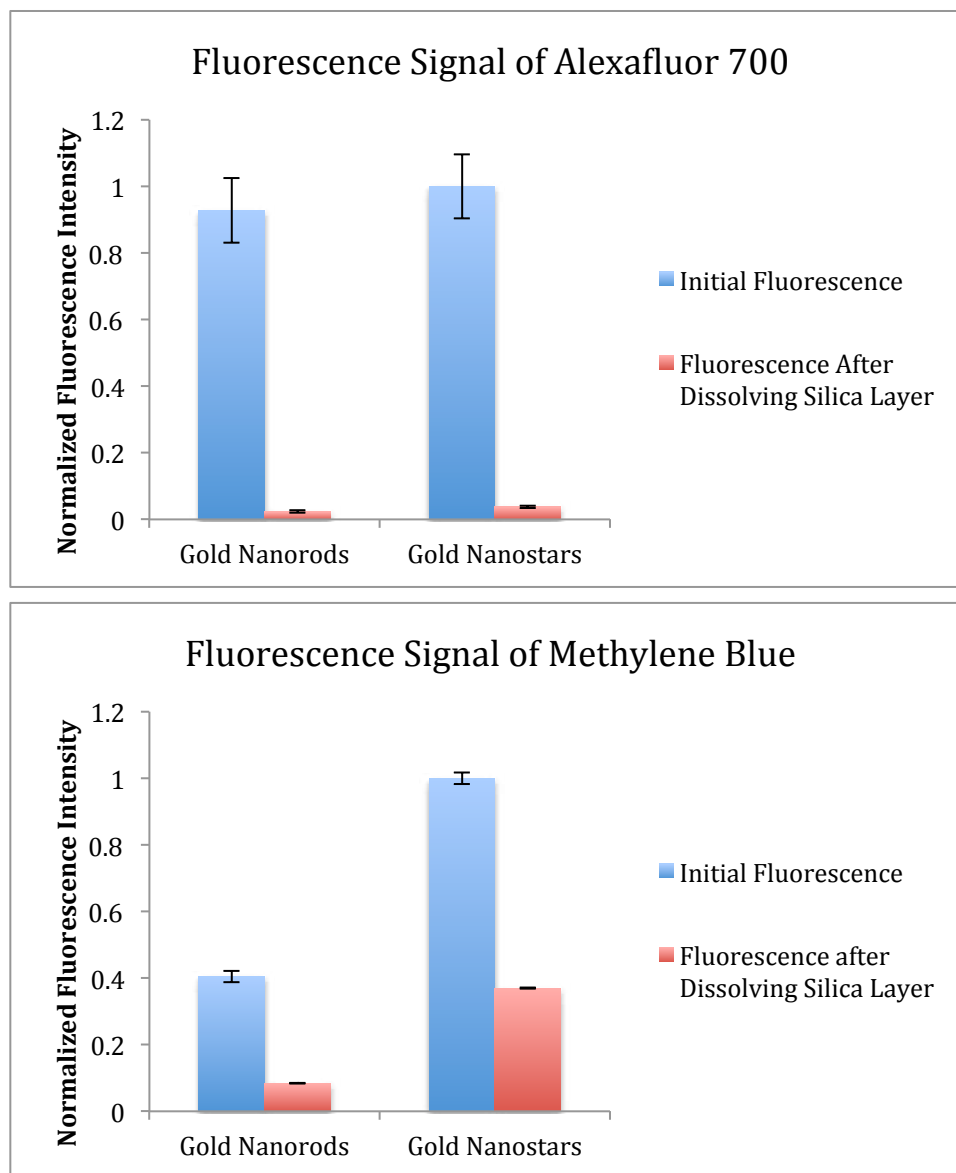
**Figure 2.3** Fluorescence signal of Alexafluor 700 (top) and methylene blue (bottom) doped into silica layer surrounding AuNS and AuNT before and after dissolving silica layer.


The initial and final fluorescence of Alexafluor 700 and methylene blue can be related to a concentration of the dyes with a calibration curve. Figure 2.4 shows the calibration curve and linear range of Alexafluor 700 and Figure 2.5 shows the calibration curve and linear range of methylene blue.
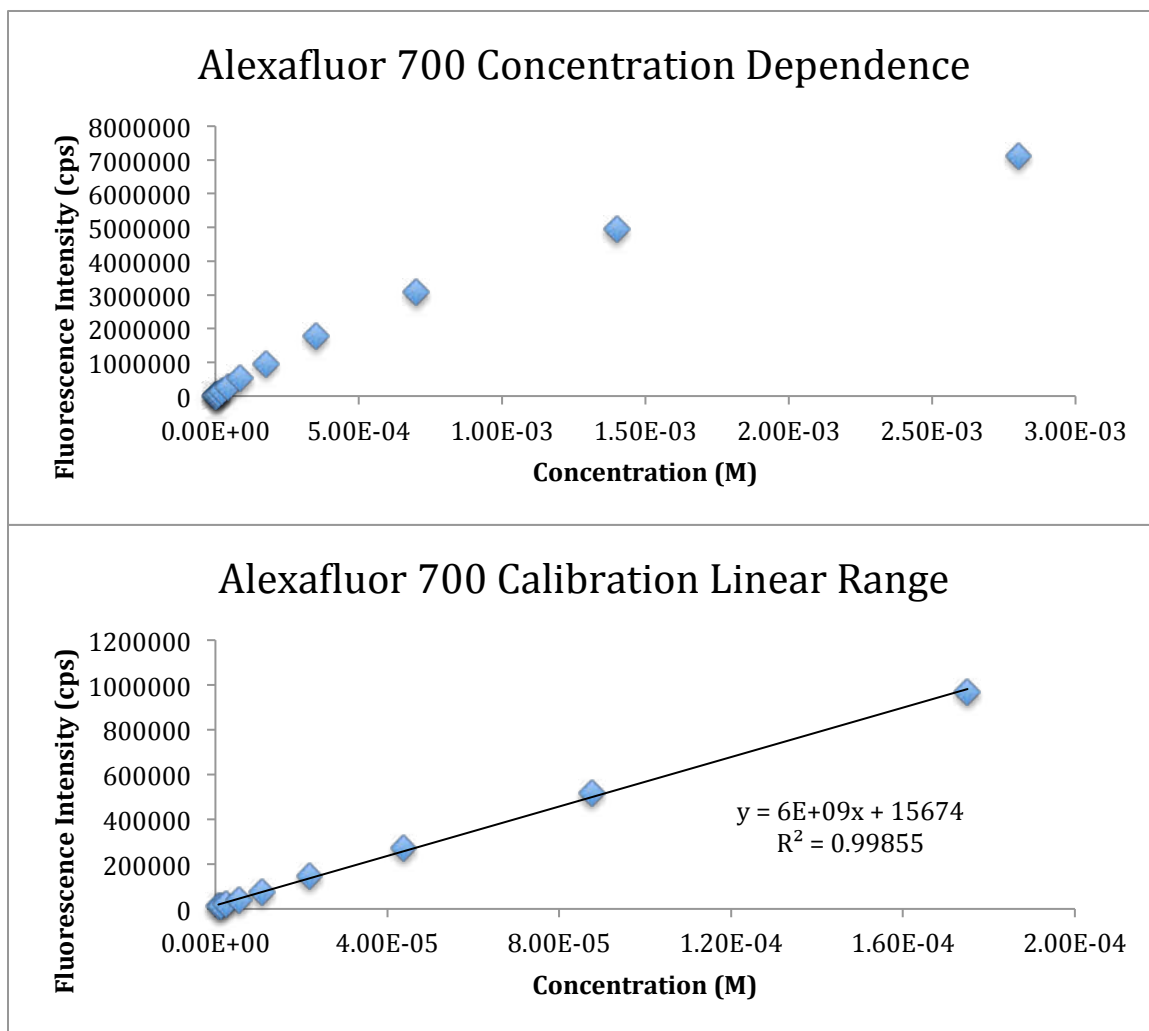
**Figure 2.4** Top: Calibration curve of Alexafluor 700. Bottom: Linear range of calibration curve. The line of best fit was found to be y = 6E+09x + 15674 using least squares method.
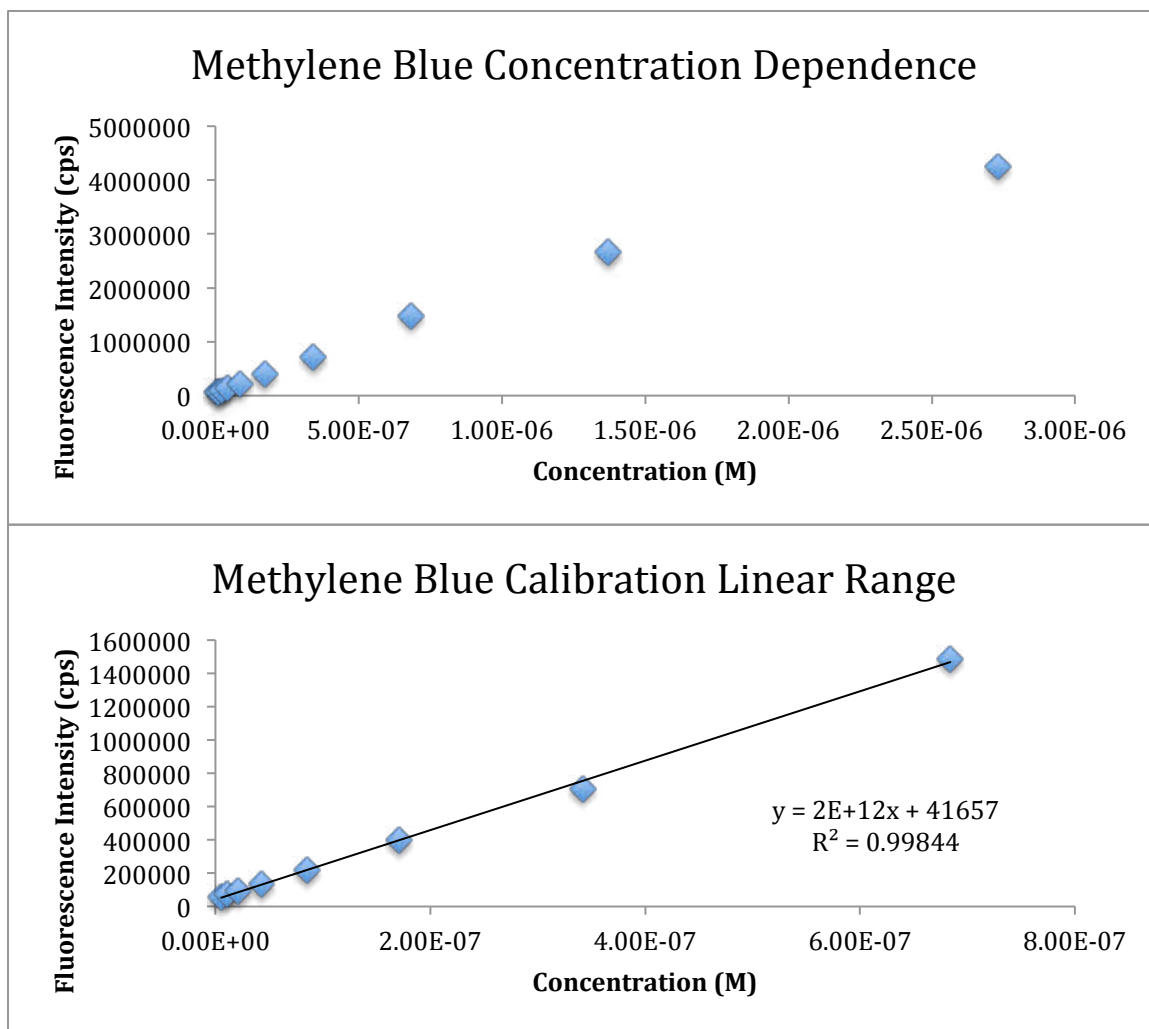
**Figure 2.5** Top: Calibration curve of methylene blue. Bottom: Linear range of calibration curve. The line of best fit was found to be y = 2E+12x + 41657 using least squares method.

From the linear ranges of the calibration curves and the line of best fit, it is possible to calculate the concentration of fluorescent dye that was trapped in the silica layer. It is also possible to calculate the theoretical concentration of the dye under enhanced fluorescence conditions.

Table 2.2 shows the results of the calculations.

|  | Average Initial Fluorescence (cps) | Average Fluorescence after Silica Layer was Dissolved (cps) |
|---|---|---|
| Alexafluor 700 |  |  |
| AuNR | $1.5 * 10^6$ | $3.9 * 10^4$ |
| AuNS | $1.6 * 10^6$ | $6.2 * 10^4$ |
| Methylene Blue |  |  |
| AuNR | $1.0 * 10^6$ | $2.1 * 10^5$ |
| AuNS | $2.5 * 10^6$ | $9.3 * 10^5$ |

|  | Average Calculated Theoretical Concentration From Initial Fluorescence (M) | Average Trapped Dye Concentration (M) |
|---|---|---|
| Alexafluor 700 |  |  |
| AuNR | $2.5 * 10^{-4}$ | $3.9 * 10^{-6}$ |
| AuNS | $2.7 * 10^{-4}$ | $7.8 * 10^{-6}$ |
| Methylene Blue |  |  |
| AuNR | $4.9 * 10^{-7}$ | $8.5 * 10^{-8}$ |
| AuNS | $1.2 * 10^{-6}$ | $4.4 * 10^{-7}$ |

**Table 2.2** The initial fluorecence and fluorescence after dissolving silica layer was measured and reported for both AuNR and AuNS with Alexafluor 700 and methylene blue. The calculated concentration for all fluorescence measurements was done with the calibration equation for the appropriate fluorescent dye.

**Table 2.2** shows the calculated concenctions of the dyes before and after the silica layer was dissolved.  The initial concentration of each dye added to solution during silica layer growth was 0.0255 M.  It is found that the concentration of dye trapped in the silica layer is several orders of magnitude less than that. It is also possible to calculate a fluorescence enhancement factor, F (F=$I_{nanocomposites}$/$I_{released dye}$, $I_{nanocomposites}$ is the fluorescence intensity of dye-doped nanocomposites; $I_{released dye}$ is the fluorescence intensity of released dye).

Table 2.3 shows the calculated fluorescence enhancement factor for AuNR and AuNS with Alexafluor 700 and methylene blue.

| | Fluorescence Enhancement Factor |
|---|---|
| Alexafluor 700 | |
| AuNR | 38.5 |
| AuNS | 25.8 |
| Methylene Blue | |
| AuNR | 4.8 |
| AuNS | 2.7 |

**Table 2.3** Fluorescence enhancement factors for AuNR and AuNS with each dye.

Table 2.3 shows the fluorescence enhancement factors. It can be seen that the enhancement factor for Alexafluor 700 is about 10 times larger than that for methylene blue. This is perhaps due to the the excitation of Alexafluor 700 at 680 nm, which is close to the maximum absorbance peak of AuNR at about 710 nm and the increasing absorbance of AuNS from 600 nm and beyond.  The excitation peak of Alexafluor 700 is closer to the maximum absorbance values for AuNR and AuNS than the excitation peak of methylene blue at 665 nm.

It was expected that the AuNS would have larger fluorescence enhancement than AuNR due to the more complicated three-dimensional shape that allows for greater interaction of the plasmon modes. However, it was observed that the fluorescence enhancement of AuNS was less than that of AuNR, possibly due to low yield of silica covered particles or particle aggregation.

2.3.4 Characterization of Silica Coated Nanoparticles

The silica coated nanoparticles were characterized with STEM images. In the images shown in Figure 2.6, the AuNR and AuNS are seen as dark grey/black with a ligher grey area around them indicating the silica layer.
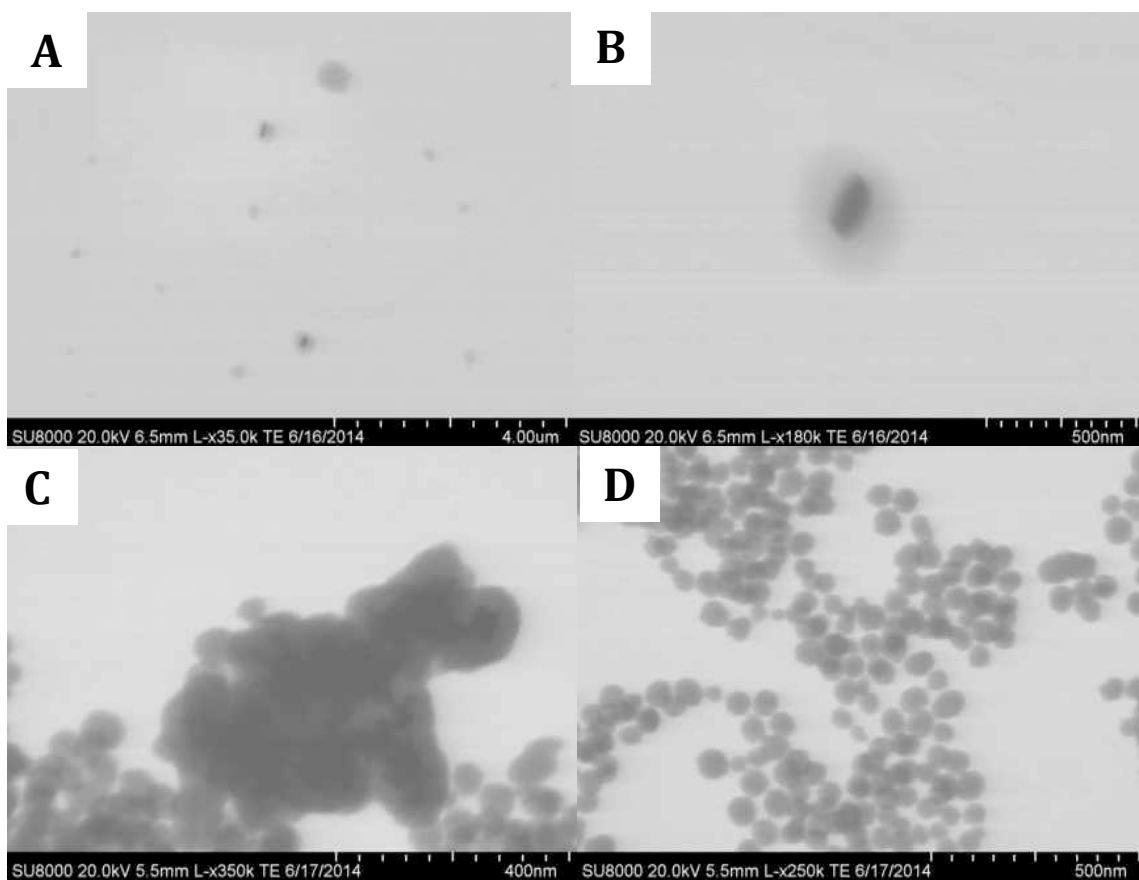
**Figure 2.6** (A) Image showing two silica coated AuNR. (B) More magnified image of silica coated AuNR. (C) Aggregated cluster of AuNS. (D) Silica nanoparticles from same sample as AuNS.

Figure 2.6 shows the STEM images. From the images, it was concluded that very low yields of silica coated nanoparticles were achieved. In both cases, greater yields of spherical silica nanoparticles were found. In Figure 2.6 (C), a large cluster of AuNS coated with silica was found, indicating that aggregation of the AuNS is a problem that could have contributed to lower than expected fluorescence results.

2.4 Conclusions

Fluorescence enhancement of AuNR and AuNS was measured with two different fluorescent dyes. Results were unexpected and showed that further investigation must be done. It was seen that AuNR gave greater fluorescence enhancement for both dyes, although AuNS were expected to give higher enhancement due to their three-dimensionsal structure with more highly interacting plasmon modes. Alexafluor 700 showed greater fluorescence enhancement with both types of nanostructures, possibly due to excitation wavelength of 680 which is closer to the maximum absorbance for both nanostructures than the excitation wavelength of methylene blue at 665 nm. For better results in the future, optimization of silica layer growth must be done to increase yield of silica coated gold nanoparticles and limit growth of pure silica nanoparticles.

REFERENCES

1.     Fort, E.; Gresillon, S. Surface enhanced fluorescence. *J. Phys. D: Appl. Phys.* **2007**, *41*, 1 – 31.

2.     Rather, H. *Surfaces Plasmons on Smooth and Rough Surfaces and on Gratings: Springer Tracts in Modern Physics,* vol 111; Springer: Berlin, 1988.

3.     University of Victoria Advanced Imaging Laboratory Jabłoński diagram. http://web.uvic.ca/ail/techniques/epi-fluorescence.html (Accessed 26 August 2012).

4.      Lajos, G.; Jancura, D.; Miskovsky, P.; Garcia-Ramos, J.V.; Sanchez-Cortes, S. Surface-Enhanced Fluorescence and Raman Scattering Study of Antitumoral Drug Hypericin: An Effect of Aggregation and Self-Spacing Depending on pH. *J. Phys. Chem. C* **2008**, *112*, 12974 – 12980.

5.     Dielectric Constants Chart. http://www.asiinstr.com/technical/Dielectric%20Constants.htm (accessed 25 August 2012).

6.     Beaglehole, D.; De Crescenzi, M. Dielectric Constant of Gold, Copper, and Gold-Copper alloys between 18 and 35 eV. *Phys. Rev. B* **1979**, *19*, 6303 – 6314.

7.     Stoller, P.; Jacobsen, V.; Sandoghdar, V. Measurement of the complex dielectric constant of a single gold nanoparticle. *Opt. Lett.* **2006**, *31*, 2474 – 2476.

8.      Zhang, Y. F.; Tang, Y. H.; Wang, N.; Yu, D. P.; Lee, C. S.; Bello, I.; Lee, S. T. Silicon nanowires prepared by laser ablation at high temperature. *Appl. Phys, Lett.***1998**, *72*, 1835-1837.

9.      Sivakov, V.; Andra, G.; Gawlik, A.; Berger, A.; Plentz, J.; Falk, F.; Christiansen, S. H. Silicon nanowire-based solar cells on glass: synthesis, optical properties, and cell parameters. *Nano Lett.* **2009**, *9*, 1549-1554.

10.     Paska, Y.; Stelzner, T.; Christiansen, S.; Haick, H. Enhanced sensing of nonpolar volatile organic compounds by silicon nanowire field effect transistors. *ACS Nano* **2011**, *5*, 5620-5626.

11.     Zheng, G.; Gao, X. P.; Lieber, C. M. Frequency domain detection of biomolecules using silicon nanowire biosensors. *Nano Lett.* **2010**, *10*, 3179-3183.

12.     Devarapalli, R. R.; Shinde, D. R.; Barka-Bouaifel, F.; Yenchalwar, S. G.; Boukherroub, R.; More, M. A.; Shelke, M. V. Vertical arrays of SiNWs-ZnO nanostructures as high performance electron field emitters. *J. Mat. Chem.* **2012**, *22*, 22922-22928.

13.     Cui, Y.; Wei, Q.; Park, H.; Lieber, C. M. Nanowire nanosensors for highly sensitive and selective detection of biological and chemical species. *Science* **2001**, *293*, 1289-1292.

14.     Chen, L. J. Silicon nanowires: the key building block for future electronic devices. *J. Mat. Chem.* **2007**, *17*, 4639.

15.     Teo, B. K.; Sun, X. H. Silicon-based low-dimensional nanomaterials and nanodevices. *Chem. Rev.* **2007**, *107*, 1454-1532.

16. Tilke, A. T.; Simmel, F. C.; Lorenz, H.; Blick, R. H.; Kotthaus, J. P. Quantum interference in a one-dimensional silicon nanowire. *Phys. Rev. B* **2003**, *68*, 075311.

17. Pavesi, L.; Dal Negro, L.; Mazzoleni, C.; Franzo, G.; Priolo, F. Optical gain in silicon nanocrystals. *Nature* **2000**, *408*, 440-444.

18. Bashouti, M. Y.; Stelzner, T.; Christiansen, S.; Haick, H. Covalent Attachment of Alkyl Functionality to 50 nm Silicon Nanowires through a Chlorination/Alkylation Process. *J. Phys. Chem. C* **2009**, *113*, 14823-14828.

19. Cui, Y.; Zhong, Z.; Wang, D.; Wang, W. U.; Lieber, C. M. High Performance Silicon Nanowire Field Effect Transistors. *Nano Lett.* **2003**, *3*, 149-152.

20. Gao, Z.; Agarwal, A.; Trigg, A. D.; Singh, N.; Fang, C.; Tung, C. H.; Fan, Y.; Buddharaju, K. D.; Kong, J. Silicon nanowire arrays for label-free detection of DNA. *Anal. Chem.* **2007**, *79*, 3291-3297.

21. Peng, K. Q.; Lee, S. T. Silicon nanowires for photovoltaic solar energy conversion. *Adv. Mater.* **2011**, *23*, 198-215.

22. Ma, D. D.; Lee, C. S.; Au, F. C.; Tong, S. Y.; Lee, S. T. Small-diameter silicon nanowire surfaces. *Science* **2003**, *299*, 1874-1877.

23. Choi, Y.-K.; Zhu, J.; Grunes, J.; Bokor, J.; Somorjai, G. A. Fabrication of Sub-10-nm Silicon Nanowire Arrays by Size Reduction Lithography. *J. Phys. Chem. B* **2003**, *107*, 3340-3343.

24. Patolsky, F.; Zheng, G.; Lieber, C. M. Fabrication of silicon nanowire devices for ultrasensitive, label-free, real-time detection of biological and chemical species. *Nature Protocols* **2006**, *1*, 1711-1724.

25.	Huang, Z.; Fang, H.; Zhu, J. Fabrication of Silicon Nanowire Arrays with Controlled Diameter, Length, and Density. *Advanced Materials* **2007**, *19*, 744-748.

26.	Schmidt, V.; Wittemann, J. V.; Senz, S.; Gösele, U. Silicon Nanowires: A Review on Aspects of their Growth and their Electrical Properties. *Advanced Materials* **2009**, *21*, 2681-2702.

27.	Geyer, N.; Fuhrmann, B.; Leipner, H. S.; Werner, P. Ag-mediated charge transport during metal-assisted chemical etching of silicon nanowires. *ACS Appl. Mater. Interfaces* **2013**, *5*, 4302-4308.

28.	Hannon, J. B.; Kodambaka, S.; Ross, F. M.; Tromp, R. M. The influence of the surface migration of gold on the growth of silicon nanowires. *Nature* **2006**, *440*, 69-71.

29.	Schmidt, V.; Wittemann, J. V.; Gosele, U. Growth, thermodynamics, and electrical properties of silicon nanowires. *Chem. Rev.* **2010**, *110*, 361-388.

30.	Chen, W.; Yao, H.; Tzang, C. H.; Zhu, J.; Yang, M.; Lee, S.-T. Silicon nanowires for high-sensitivity glucose detection. *Appl. Phys. Lett.* **2006**, *88*, 213104.

31.	Li, Z.; Chen, Y.; Li, X.; Kamins, T. I.; Nauka, K.; Williams, R. S. Sequence-Specific Label-Free DNA Sensors Based on Silicon Nanowires. *Nano Lett.* **2004**, *4*, 245-247.

32.    Feng, X. L.; He, R.; Yang, P.; Roukes, M. L. Very High Frequency Silicon Nanowire Electromechanical Resonators. *Nano Lett.* **2007**, *7*, 1953-1959.

33. He, Y.; Su, S.; Xu, T.; Zhong, Y.; Zapien, J. A.; Li, J.; Fan, C.; Lee, S.-T. Silicon nanowires-based highly-efficient SERS-active platform for ultrasensitive DNA detection. *Nano Today* **2011**, *6*, 122-130.

34.    Mu, L.; Shi, W.; Chang, J. C.; Lee, S. T. Silicon nanowires-based fluorescence sensor for Cu(II). *Nano Lett.* **2008**, *8*, 104-109.

35.    Chan, C. K.; Peng, H.; Liu, G.; McIlwrath, K.; Zhang, X. F.; Huggins, R. A.; Cui, Y. High-performance lithium battery anodes using silicon nanowires. *Nat. Nano* **2008**, *3*, 31-35.

36.    Xie, C.; Jie, J.; Nie, B.; Yan, T.; Li, Q.; Lv, P.; Li, F.; Wang, M.; Wu, C.; Wang, L.; Luo, L. Schottky solar cells based on graphene nanoribbon/multiple silicon nanowires junctions. *Appl. Phys. Lett.* **2012**, *100*, 193103.

37.    Suspène, C. m.; Barattin, R. g.; Celle, C.; Carella, A.; Simonato, J.-P. Chemical Functionalization of Silicon Nanowires by an Electroactive Group: A Direct Spectroscopic Characterization of the Hybrid Nanomaterial. *J. Phys. Chem. C* **2010**, *114*, 3924-3931.

38.    Sun, Q. Y.; de Smet, L. C.; van Lagen, B.; Giesbers, M.; Thune, P. C.; van Engelenburg, J.; de Wolf, F. A.; Zuilhof, H.; Sudholter, E. J. Covalently attached monolayers on crystalline hydrogen-terminated silicon: extremely mild attachment by visible light. *J. Am. Chem. Soc.* **2005**, *127*, 2514-2523.

39. Yaman, M.; Khudiyev, T.; Ozgur, E.; Kanik, M.; Aktas, O.; Ozgur, E. O.; Deniz, H.; Korkut, E.; Bayindir, M. Arrays of Indefinitely Long Uniform Nanowires and Nanotubes. *Nat. Mater.* **2011**, *10*, 494 – 501.

40. Uesawa, N.; Inasawa, S.; Tsuji, Y.; Yamaguchi, Y. Gas-Phase Synthesis of Rough Silicon Nanowires via the Zinc Reduction of Silicon Tetrachloride. *J. Phys. Chem. C* **2010**, *114*, 4291 – 4296.

41. Qu, Y.; Liao, L.; Li, Y.; Zhang, H.; Huang, Y.; Duan, X. Electrically Conductive and Optically Active Porous Silicon Nanowires. *Nano Lett.* **2009**, *9*, 4539 – 4543.

42. Chen, H.; Xu, J.; Chen, P.; Fang, X.; Qiu, J.; Fu, Y.; Zhou, C. Bulk Synthesis of Crystalline and Crystalline Core/Amorphous Shell Silicon Nanowires and Their Application for Energy Storage. *ACS Nano* **2011**, *5*, 8383 – 8390.

43. Kim, B.; Koo, T.; Lee, J.; Kim, D.S.; Jung, Y.C.; Hwang, S.W.; Choi, B.L.; Lee, E.K.; Kim, J.M.; Whang, D. Catalyst-free Growth of Single-Crystal Silicon and Germanium Nanowires. *Nano Lett.* **2009**, *9*, 864 – 869.

44. Hochbaum, A.I.; Gargas, D.; Hwang, Y.J.; Yang, P. Single Crystalline Mesoporous Silicon Nanowires. *Nano Lett.* **2009**, *9*, 3550 – 3554.

45. Yuan, F.; Tuan, H. Supercritical Fluid-Solid Growth of Single-Crystalline Silicon Nanowires: An Example of Metal-Free Growth in an Organic Solvent. *Cryst. Growth Des.* **2010**, *10*, 4741 – 4745.

46. Wang, H.Q.; Wang, G.Z.; Jia, L.C.; Tang, J.; Li, G.H. Catalyst Synthesis of Silicon-Based $Zn_2SiO_4$-$SiO_x$ Heterostructure Nanowires. *J. Phys. Chem. C* **2007**, *111*, 14307 – 14311.

47. Streetman, B.G.; Banerjee, S. *Solid State Electronic Devices*, 5th ed.; Prentice Hall: New Jersey, 2000.

48. Jin, Y.; Friedman, N. Surface Plasmon Resonance-Mediated Colloid Gold Monolayer Junctions. *J. Am. Chem. Soc*. **2005**, *127*, 11902 – 11903.

49. Wu, Z.; Jin, R. On the Ligand's Role in the Fluorescence of Gold Nanoclusters. *Nano Lett*. **2010**, *10*, 2568 – 2573.

50. Shao, L.; Woo, K.C.; Chen, H.; Jin, Z.; Wang, J.; Lin, H. Angle- and Energy-Resolved Plasmon Coupling in Gold Nanorod Dimers. *ACS Nano* **2010**, *4*, 3053 – 3062.

51. Ringe, E.; Langille, M.R.; Sohn, K.; Zhang, J.; Huang, J.; Mirkin, C.A.; Van Duyne, R.P.; Marks, L.D. Plasmon Length: A Universal Parameter to Describe Size Effects in Gold Nanoparticles. *J. Phys. Chem. Lett*. **2012**, *3*, 1497 – 1483.

52. Luo, B.; Wang, B.; Liang, M.; Ning, J.; Li, X.; Zhi, L. Reduced graphene oxide-mediated growth of uniform tin-core/carbon-sheath coaxial nanocables with enhanced lithium ion storage properties. *Adv. Mater.* **2012**, *24*, 1405-1409.

53. Minati, L.; Antonini, V.; Dalla Serra, M.; Speranza, G. Multifunctional branched gold-carbon nanotube hybrid for cell imaging and drug delivery. *Langmuir* **2012**, *28*, 15900-15906.

54. Oosterhout, S. D.; Wienk, M. M.; van Bavel, S. S.; Thiedmann, R.; Koster, L. J.; Gilot, J.; Loos, J.; Schmidt, V.; Janssen, R. A. The effect of three-dimensional morphology on the efficiency of hybrid polymer solar cells. *Nat. Mater.* **2009**, *8*, 818-824.

55. Jiang, Y.; Wang, H.-Y.; Wang, H.; Gao, B.-R.; Hao, Y.-w.; Jin, Y.; Chen, Q.-D.; Sun, H.-B. Surface Plasmon Enhanced Fluorescence of Dye Molecules on Metal Grating Films. *J. Phys. Chem. C* **2011**, *115*, 12636-12642.

56. Zhuo, S.; Shao, M.; Xu, H.; Chen, T.; Ma, D. D. D.; Lee, S.-T. Au-modified silicon nanowires for surface-enhanced fluorescence of Ln3+ (Ln = Pr, Nd, Ho, and Er). *J. Mat. Sci* **2012**, *24*, 324-330.

57. Lajos, G.; Jancura, D.; Miskovsky, P.; García-Ramos, J. V.; Sanchez-Cortes, S. Surface-Enhanced Fluorescence and Raman Scattering Study of Antitumoral Drug Hypericin: An Effect of Aggregation and Self-Spacing Depending on pH. *J. Phys. Chem. C* **2008**, *112*, 12974-12980.

58. Hwang, E.; Smolyaninov, II; Davis, C. C. Surface plasmon polariton enhanced fluorescence from quantum dots on nanostructured metal surfaces. *Nano Lett.* **2010**, *10*, 813-820.

59. Medintz, I. L.; Uyeda, H. T.; Goldman, E. R.; Mattoussi, H. Quantum dot bioconjugates for imaging, labelling and sensing. *Nat. Mater.* **2005**, *4*, 435-446.

60. Wu, Z.; Jin, R. On the ligand's role in the fluorescence of gold nanoclusters. *Nano Lett.* **2010**, *10*, 2568-2573.

61. Shao, L.; Woo, K. C.; Chen, H.; Jin, Z.; Wang, J.; Lin, H. Q. Angle- and energy-resolved plasmon coupling in gold nanorod dimers. *ACS Nano* **2010**, *4*, 3053-3 062.

62. Zhang, J.; Lakowicz, J. R. A model for DNA detection by metal-enhanced fluorescence from immobilized silver nanoparticles on solid substrate. *J.Phys. Chem. B* **2006**, *110*, 2387-2392.

63.  Ray, K.; Badugu, R.; Lakowicz, J. R. Metal-enhanced fluorescence from CdTe nanocrystals: a single-molecule fluorescence study. *J. Am. Chem. Soc.* **2006**, *128*, 8998-8999.

64.  Jie, Y.; Yonghua, L.; Pei, W.; Hai, M. Integral fluorescence enhancement by silver nanoparticles controlled via PMMA matrix. *Optics Communications* **2011**, *284*, 494-497.

65.  Aslan, K.; Lakowicz, J. R.; Szmacinski, H.; Geddes, C. D. Metal-Enhanced Fluorescence Solution-Based Sensing Platform. *Journal of Fluorescence* **2004**, *14*, 677-679.

66.  Guerrero, A. R.; Aroca, R. F. Surface-enhanced fluorescence with shell-isolated nanoparticles (SHINEF). *Angew Chem Int Ed Engl* **2011**, *50*, 665-668.

67.  Li, J. F.; Huang, Y. F.; Ding, Y.; Yang, Z. L.; Li, S. B.; Zhou, X. S.; Fan, F. R.; Zhang, W.; Zhou, Z. Y.; WuDe, Y.; Ren, B.; Wang, Z. L.; Tian, Z. Q. Shell-isolated nanoparticle-enhanced Raman spectroscopy. *Nature*, *464*, 392-395.

68.  Zhang, J.; Lakowicz, J. R. Metal-enhanced fluorescence of an organic fluorophore using gold particles. *Optics Express* **2007**, *15*, 2598-2906.

69.  Jain, P. K.; El-Sayed, M. A. Universal scaling of plasmon coupling in metal nanostructures: extension from particle pairs to nanoshells. *Nano Lett.* **2007**, *7*, 2854-2858.

70.  Jain, P. K.; El-Sayed, M. A. Surface Plasmon Coupling and Its Universal Size Scaling in Metal Nanostructures of Complex Geometry: Elongated Particle Pairs and Nanosphere Trimers. *J. Phys. Chem. C* **2008**, *112*, 4954-4960.

71.    Fischer, K. E.; Aleman, B. J.; Tao, S. L.; Hugh Daniels, R.; Li, E. M.; Bunger, M. D.; Nagaraj, G.; Singh, P.; Zettl, A.; Desai, T. A. Biomimetic nanowire coatings for next generation adhesive drug delivery systems. *Nano Lett.* **2009**, *9*, 716-720.

72.    Lee, S. H.; Rusakova, I.; Hoffman, D. M.; Jacobson, A. J.; Lee, T. R. Monodisperse SnO2-coated gold nanoparticles are markedly more stable than analogous SiO2-coated gold nanoparticles. *ACS Appl. Mater. Interfaces* **2013**, *5*, 2479-2484.

73.    Yang, H.; Nagai, K.; Abe, T.; Homma, H.; Norimatsu, T.; Ramaraj, R. Enhanced catalytic activity of gold nanoparticles doped in a mesoporous organic gel based on polymeric phloroglucinol carboxylic acid-formaldehyde. *ACS Appl. Mater. Interfaces* **2009**, *1*, 1860-1864.

74.    Zhang, J.; Malicka, J.; Gryczynski, I.; Lakowicz, J. R. Surface-enhanced fluorescence of fluorescein-labeled oligonucleotides capped on silver nanoparticles. *J. Phys. Chem. B* **2005**, *109*, 7643-7648.

75.    Su, Y.; Wei, X.; Peng, F.; Zhong, Y.; Lu, Y.; Su, S.; Xu, T.; Lee, S. T.; He, Y. Gold nanoparticles-decorated silicon nanowires as highly efficient near-infrared hyperthermia agents for cancer cells destruction. *Nano Lett.* **2012**, *12*, 1845-1850

76.    Fort, E.; Gresillon, S. Surface Enhanced Fluorescence. *J. Phys. D: Appl. Phys.* **2007**, *41*, 1 − 31.

77.    Xie, J.; Lee, J. Y.; Wang, D. I. C. Seedless, Surfactantless, High-Yield Synthesis of Branched Gold Nanocrystals in HEPES Buffer Solution. *Chem. Mater.* **2007**, *19*, 2823 − 2830.

78.     Yuan, H.; Ma, W.; Chen, C.; Zhu, H.; Gao, X.; Zhao, J. Controllable Synthesis of 3D Thorny Plasmonic Gold Nanostructures and Their Tunable Optical Properties. *J. Phys. Chem. C* **2011**, *115*, 23256 – 23260.

79.     Smith, D. K.; Miller, N. R.; Korgel, B. A. Iodide in CTAB Prevents Gold Nanorod Formation. *Langmuir*, **2009**, 9518 – 9524.

80.     Navarro, J.; Liotta, A.; Faure, A.-C.; Lerouge, F.; Chaput, F.; Micouin, G.; Baldeck, P. L.; Parola, S. Tuning dye-to-particle interactions towards luminescent gold nanostars. *Langmuir*, **2013**, ASAP.

81.     Hurst, S. J.; Jean-Lytton, A. K. R.; Mirkin, C. A. Maximizing DNA Loading on a Range of Gold Nanoparticle Sizes. *Anal. Chem.* **2006**, *78*, 8313 – 8318.

82.     Shiotani, A.; Akiyama, Y.; Kawano, T.; Niidome, Y.; Mori, T.; Katayana, Y.; Niidome, T. Active Accumulation of Gold Nanorods in Tumor in Response to Near-Infrared Laser Irradiation. *Bioconjugate Chem*. **2010**, *21*, 2049 – 2054.

83.     Stöber, W.; Fink, A.; Bohn, E. J. Controlled Growth of Monodisperse Silica Spheres in the Micron Size Range. *Colloid Interface Sci.* **1968**, *16*, 62 – 69.

84.     Chen, J.; Jin, Y.; Fahruddin, N.; Zhao, J. X. Development of Gold Nanoparticle-Enhanced Fluorescent Nanocomposites. *Langmuir*, **2013**, *29*, 1584 – 1591.

85.     Jain, P. K.; Lee, K. S.; El-Sayed, I. H.; El-Sayed, M. A. Calculated Absorption and Scattering Properties of Gold Nanoparticles of Different Size, Shape and Composition: Applications in Biological Imaging and Biomedicine. *J. Phys. Chem. B* **2006**, *110,* 7238 – 7248.

86. Imura, K.; Nagahara, T.; Okamoto, H. Near-Field Two-Photon-Induced Photoluminescence from Single Gold Nanorods and Imaging of Plasmon Modes. *J. Phys. Chem. B* **2005**, *109*, 13214 – 13220.

87. Imura, K.; Nagahara, T.; Okamoto, H. Near-Field Optical Imaging of Plasmon Modes in Gold Nanorods *J. Chem. Phys.* **2005**, *122*, 154701-1 – 154791-5.

88. Imura, K.; Nagahara, T.; Okamoto, H. Plasmon Mode Imaging of Single Gold Nanorods *J. Am. Chem. Soc*. **2004**, *126*, 12730 – 12731.

89. Bouhelier, A.; Bachelot, R.; Lerondel, G.; Kostcheev, S.; Royer, P.; Wiederrecht, G. P. Surface Plasmon Characteristics of Tunable Photoluminescence in Single Gold Nanorods. *Phys. Rev. Lett*. **2005**, *95*, 267405.

90. Hao, F.; Nehl, C. L.; Hafner, J. H.; Norlander, P. Plasmon Resonances of a Gold Nanostar. *Nano Lett.* **2007**, *7*, 729 – 732.